Proceedings 10th NUMGE 2023
10th European Conference on Numerical Methods in Geotechnical Engineering
Zdravkovic L, Kontoe S, Taborda DMG, Tsiampousi A (eds)

https://doi.org/10.53243/NUMGE2023-288

Numerical modelling of liquefaction around marine structures in the OpenFOAM® framework

C. Windt[1], R. Shanmugasundaram[3], S. Schimmels[2], M. Kudella[2], H. Rusche[3], V.S.O. Kirca[4], B.M. Sumer[4], V. Vanjakula[5], F. Adam[5], D. Majewski[6], K. Kazimierowicz-Frankowska[6], M. Pietrzkiewicz[7], N. Goseberg[1,2]

[1]*Technische Universität Braunschweig, Leichtweiß-Institute for Hydraulic Engineering and Water Resources, Braunschweig, Germany*

[2]*Coastal Research Centre, Hannover, Germany*

[3]*WIKKI GmbH, Wernigerode, Germany*

[4]*BM SUMER Consultancy & Research, Istanbul, Turkey*

[5]*GICON GmbH, Rostock, Germany*

[6] *Institute of Hydro-Engineering of the Polish Academy of Sciences, Gdansk, Poland*

[7] *PROJMORS Designing Office for Maritime Structures Co. Ltd., Gdansk, Poland*

ABSTRACT: Enhanced understanding of the wave-induced response of the seabed around marine structures is essential for a more efficient exploitation of marine resources. Depending on the prevailing conditions, the seabed response can result in soil liquefaction, leading to catastrophic failure of marine structures. Therefore, accurate and efficient numerical models of wave-structure-soil interaction, capturing the hydrodynamic, structural, and geotechnical processes, are necessary for an optimised development of marine infrastructure. The project "Numerical modelling of liquefaction around marine structures" aims at developing an open-source numerical modelling framework for liquefaction around marine structures. This paper will present the state-of-the-art of numerically modelling the wave-induced seabed response and liquefaction. Furthermore, the paper will lay out the unique modelling framework for the entire liquefaction process, implemented in OpenFOAM®, and provide details on the calibration and validation strategy using small and large scale experiments, respectively. Initial numerical results are shown for different stages of the liquefaction sequence, indicating promising agreement with reference data from the literature.

Keywords: Liquefaction; OpenFOAM®; Wave-Structure-Soil Interaction; Marine Structures; Floating Offshore Wind

1 INTRODUCTION

The importance of an increase exploitation of marine renewable energy sources is highlighted by the recent geo-political events with their impact on energy security and pricing, together with the global efforts to mitigate the anthropogenic climate change (e.g. by fostering the production of green hydrogen). It is well known that offshore wind, with its trend towards floating installations of >12 MW (see Figure 1), is a considerable driver of the expansion of marine renewable energy harvesting. Next to the required research and development of novel turbines, generators, and towers, the sub-sea components (floating substructure, mooring, anchoring) need to be innovated to follow future trends.

For the anchoring, geotechnical challenges, such as scour and seabed liquefaction, have been identified. Seabed liquefaction in particular can lead to severe failure of marine structures (Bjerrum, 1973).

Figure 1: Rendering of GICON®'s tension leg platform (TLP)-type concept (courtesy of GICON®)

1.1 Seabed liquefaction

Seabed soil can lose its bearing capacity when pore pressure accumulates. Such an accumulation is triggered by cyclic shear stress induced, for instance, by seismic loading or cyclic surface wave action.

When applying shear stress on a volume of loosely packed soil (
Figure 2 (a)), the soil grains show a tendency to rearrange and contract, resulting in a decrease of pore volume in-between the grains. The decrease of the pore volume leads to an increase in pore pressure and, in turn, a tendency of the pore water to flow out of the pore volume. If the soil volume is able to drain, the increased pore pressure dissipates (Figure 2 (b.1)). In undrained conditions, when the pore pressure cannot dissipate, it accumulates (
Figure 2 (b.2)). Following Terzaghi's principle, the increased pore pressure results in a reduction of the normal effective stress in the soil volume up to a point where the soil effectively loses its bearing capacity – it liquefies (
Figure 2 (c))[1].

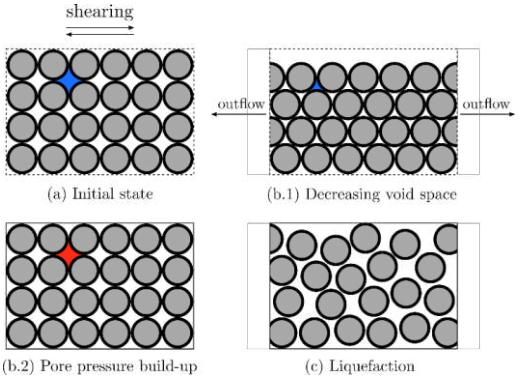

Figure 2: Schematic representation of the physical processes leading to seabed liquefaction. (Figure adapted from (Sumer et al., 2006))

After liquefaction, a pore pressure gradient triggers the settling of soil grains, resulting in the change of state from liquid to solid soil (i.e. compaction).

The prediction and analysis of the geotechnical processes leading to and resulting from seabed liquefaction is complex and mostly relies on experimental and numerical modelling approaches. While physical model tests are subject to model, scale, and size effects, numerical modelling approaches can alleviate some of the existing limitations of physical models. However, the implementation of the prevailing, coupled hydro-geotechnical processes is not trivial.

This paper presents efforts to develop, calibrate, and validate a numerical model for the liquefaction in the vicinity of marine structures in the OpenFOAM® framework, including all relevant processes from pore pressure build-up to liquefaction and compaction.

[1] While liquefaction can be divided into residual and momentary liquefaction, only wave-induced residual liquefaction is subject of this paper.

2 MODELLING OF LIQUEFACTION

Considering the seabed soil as poro-elastic solid, models to describe seabed liquefaction are described by Biot's theory on poro-elasticity (Biot, 1941). Two equations are derived for the linear momentum balance and the pore fluid continuity. The total momentum balance of the poro-elastic solid is achieved when the equilibrium conditions of the stress field are satisfied:

$$\nabla \cdot \sigma = 0, \qquad \text{with } \sigma = \sigma' - pI\,. \tag{1}$$

In Eq. (1), σ' is the effective stress (carried by the soil skeleton), p is the phase-resolved pore fluid pressure, and I is the identity tensor. Applying Hooke's law, the equilibrium of poro-elastic soil can be derived as:

$$G\nabla^2 U + \frac{G}{1-2\nu}\nabla\varepsilon = \nabla p\,, \tag{2}$$

where G denotes the shear modulus, ν the Poisson ratio, U the displacement vector, and ε is the volumetric strain. The conservation of mass of pore water is formally expressed by Eq. (4), where V is the velocity vector, n is the porosity, and K' is the true bulk modulus of elasticity of water (Verruijt, 1969).

$$\frac{\partial}{\partial t}\left(\varepsilon + \frac{n}{K'}p\right) + \nabla \cdot V = 0 \tag{3}$$

Applying Darcy's law, the continuity equation for the pore water reads

$$\frac{k}{\gamma}\nabla^2 p = \frac{n}{K'}\frac{\partial p}{\partial t} + \frac{\partial \varepsilon}{\partial t}\,, \tag{4}$$

where k denotes the hydraulic conductivity and γ denotes the specific weight of the soil.

2.1 Pore pressure build up

Eqs. (2) and (4) do not cater for the build-up of the pore pressure. To that end, Sumer (2014) provides a description for the pore pressure build-up:

$$\frac{\partial P}{\partial t} = c_v \frac{\partial^2 P}{\partial z^2} + \frac{{\sigma_0}'}{N_l T}\,, \quad \text{with } N_l = \left(\frac{1}{\alpha_N}\frac{A_\tau}{{\sigma_0}'}\right)^{\frac{1}{\beta}}\,, \tag{5}$$

where P is the accumulated pore pressure, c_v is the coefficient of consolidation. The last term in Eq. (5) represents a source term to account for the accumulation of pore pressure. In this source term, ${\sigma_0}'$ is the initial

mean normal effective stress, T is the wave period, and N_l the required number of cycles for liquefaction to set in. α_N and β are empirical constants (De Alba et al., 1976) and A_τ is the amplitude of the shear stress, whose calculation is further defined in Section 4.

2.2 Liquefaction criterion

Following Sumer (2014), in this paper, residual liquefaction is defined to set in when the accumulated pore pressure is larger than $\sigma_0{}'$:

$$\frac{P}{\sigma_0{}'} > 1\,. \tag{6}$$

2.3 Post-liquefaction stage

Until soil liquefaction, the soil behaves likes a poro-elastic solid. In contrast, the liquefied soil behaves like a highly viscous fluid and the whole constitutive relation changes. The liquefied soil is a two-phase flow with soil particles and water. This multiphase phase problem is uniquely approached using a drift flux model in which continuity equations and the momentum equations of the individual phases can be added. This addition gives one continuity equation and one momentum equation for the whole mixture so that the numerical instabilities from the momentum transfer can be eliminated. However, an additional equation needs to be solved for the drift flux.

The governing equations of the liquefied soil are

$$\frac{\partial \rho}{\partial t} + \nabla \cdot \rho V = 0\,, \tag{7}$$

$$\frac{\partial \rho V}{\partial t} + \nabla \cdot \rho V V = -\nabla p + \rho g - \nabla \cdot \left(\frac{\alpha}{1-\alpha}\frac{\rho_c \rho_d}{\rho} V_{dj}.V_{dj}\right)\,, \tag{8}$$

$$\frac{\partial \rho \alpha}{\partial t} + \nabla \cdot \rho V \alpha = -\nabla \cdot \rho V_{dj}\,\alpha\,, \tag{9}$$

where α is the void fraction of soil grains. ρ_c, ρ_d, ρ are the densities of continous phase (water), discrete phase (soil), and mixture, respectively. V_{dj} is the drift velocity, which can be interpreted according to (Sumer, 2014) (so-called hindered settlement) as

$$V_{dj} = V_0\,(1-\alpha)^q\,. \tag{10}$$

2.4 Soil Compaction

As the pore pressure builds up, an upward-directed pressure gradient is generated, such that the accumulated pressure is largest at the impermeable base and smallest at the mudline, hence generating an upward-directed pressure gradient. This pressure gradient drives the water in the liquefied soil upwards, while the soil grains settle through the water until they begin to get into contact with each other. This process is known as soil compaction. The behaviour of the bed changes from essentially liquid in the upper layer to essentially solid (soil is denser) in the lower layer. There will be no change in pore pressure buildup after liquefaction until compaction occurs. As the soil particles settle down, α increases towards the impermenable base. The compaction criteria can be defined following Eq. (11), where n_c is the porosity of the compacted soil.

$$\alpha > 1 - n_c \tag{11}$$

3 LITERATURE REVIEW

Numerous analytical, numerical, experimental, and field studies concerning various aspects of seabed liquefaction can be found in the literature (Jeng (2003), Sumer (2014a), Sumer and Kirca (2021)).

Based on Biot's poro-elasticity theory, a number of numerical models have been developed to analyse seabed dynamics. Such models, generally, deliver higher accuracy compared to analytical models; however, require more computational effort. In his review, Jeng (2003) differentiates between numerical models based on finite differences (FD), finite elements (FE), and the boundary element method (BEM).

Early models have been developed by, e.g., Zienkiewicz et al. (1980), Sakai (1988), and Raman-Nair and Sabin (1991). While these early models focus more on the process level of seabed dynamics and liquefaction, more recently, engineering problems, by means of wave-structure-soil interaction (WSSI), are considered. Dunn et al. (2006) use the FE method around buried pipelines. Using FD, Li and Jeng (2008) analyse wave-induced pore pressures and effective stresses near a breakwater head. Stickle et al. (2013) use FE to model WSSI around a breakwater.

Jeng et al. (2013) propose an integrated model for WSSI based on the Volume-Averaged Reynolds-Averaged Navier–Stokes (VARANS) equations to incorporate wave modelling and the dynamic Biot equations for the porous elastic seabed. Discretisation is achieved via the FE method. The model is employed for the analysis of a large-scale composite breakwater.

Also employing an integrated model with the RANS equations for the mean fluid flow (using FD) and the Biot equations for the seabed (using FE), Zhao et al. (2017) analyse the seabed response around a monopile.

Recently, also the finite-volume method is used to discretise WSSI problems. Elsafti and Oumeraci (2016) and Li et al. (2020) propose modelling frameworks, implemented in the open source CFD toolbox OpenFOAM®. Both of the numerical models can be applied to predict the onset of momentary liquefaction.

4 NUMERICAL MODELLING APPRAOCH

Even though a number of numerical models for the analysis of seabed dynamics and liquefaction are available in the literature, no comprehensive model for the entire (residual) liquefaction and compaction process is available, including pore pressure build-up, as well as the state of change from solid to liquid and back to solid is available. This shortcoming is overcome by the newly proposed numerical modelling approach.

In particular, the governing equations stated in Section 2 are implemented in order to model the complete liquefaction sequence in a domain as depicted in Figure 3. Here, three main modelling areas are defined. Ω_1 represents the time varying pressure boundary conditions, to represent the progressing gravtiy waves, with pressure magnitudes stemming from linear wave theory. For the soil, Ω_2 and Ω_3 represent the regions of solid and liquefied soil, respectively. Ω_2 is govered by the Biot consolidation equations and the pore pressure build-up, while the post liquefaction and compaction Eqs. (8) – (12) govern Ω_3.

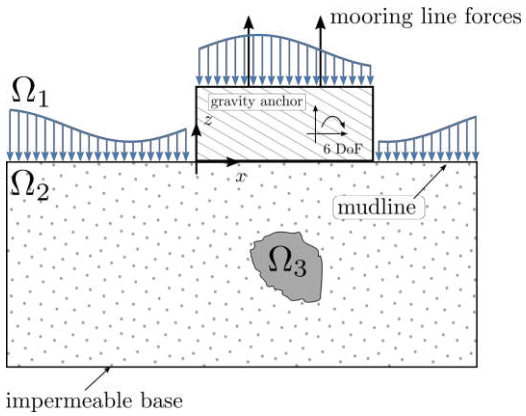

Figure 3: Schematic of the numerical setup, showing the pressure boundary conditions (Ω_1), regions of solid (Ω_2) and liquefied soil (Ω_3). (Figure adapted from (Shanmugasundaram et al., 2022)).

5 CALIBRATION & VALIDATION

In order to ensure and prove the accuracy of the numerical model, calibration and validation are essential steps during the model development.

5.1 Calibration data

For the calibration, reference data for seabed liquefaction on a process level are required, such that the required modelling coefficients (e.g. elastic moduli, Poisson's ratio, and coefficient of permeability) can be adjusted and basic model assumptions can be verified. To that end, small scale experiments in an experimental wave flume have been conducted (see Figure 4).

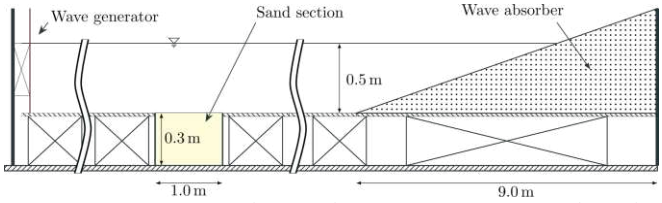

Figure 4: Experimental wave flume at IBW-PAN used for the small scale experiments.

Four different test cases, of varying complexity have been considered. First, only wave action on the seabed is considered, while the pore-pressure is measured at four specific locations in the soil pit. 19 different wave conditions with varying wave heights and periods have been tested. Retaining the hydraulic boundary conditions, next, a scaled down gravity anchor is placed on the soil pit and pore-pressure is measured again. In a third setup, wave action is omitted, while the foundation plate is excited externally by means of a rocking motion. Again pore pressure is measured in the soil pit. Finally, the settlement of the anchor is replicated by letting the foundation sink onto the soil pit with no wave action.

For the sake of brevity, the interested reader is referred to, e.g. Kazimierowicz-Frankowska et al. (2022) for results of the small scale experimental data.

5.2 Validation data

While for the model calibration fundamental model setups are required, the validation of the numerical model should be based on a realistic case study. To that end, large scale (i.e. 1/15) experiments of GICON's floating offshore wind turbine concept are planned. Similar to the small scale experiments, the sand pit is equipped with 16 pore pressure transducers to monitor pore pressure build-up and dissipation. On the sand pit, the scaled gravity anchor is placed and displacement is measure via echo-sounders. Mooring lines, equipped with force transducers, connect the gravity anchor with the floating structure. The motion of the latter is measured using the Qualisys motion tracking system. In order to realistically model the load conditions on the seabed, wind loads are induced on the system using a hardware in the loop system (Windt et al., 2022).

6 INITIAL RESULTS

In this section, numerical results for three different stages of the liquefaction process are shown, i.e. pore pressure build-up, liquefaction, and compaction.

6.1 Pore pressure build-up

As a first step, the OpenFOAM® solver *biotFoam*, which solves Eqs. (3) and (5), is verified for pore pressure and shear stress. Then the solver is extended to incorporate pore pressure build-up (Eq. (6)). The

onset of residual liquefaction is predicted using the liquefaction criteria provided in Eq. (7).

Figure 5 shows the comparison of the numerical (solid) and analytical (dashed) non-dimensional pore pressure for different time instances along the soil column. It becomes obvious that after 15 minutes, the top part of the seabed (z/h > −0.6) is completely liquefied, thereby following the analytical solution. For more details on the specific test case, the interested reader is referred to (Shanmugasundaram et al., 2022).

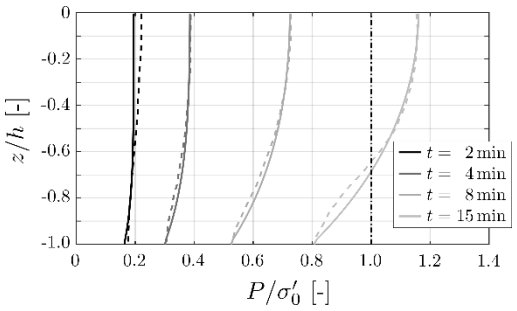

Figure 5: Comparison of the numerical (solid) and analytical (dashed) non-dimensional pore pressure. The vertical line indicates the liquefaction criterion.

6.2 Change of state: Solid to liquid

In order to perform a first test of the implementation of the phase change from solid to liquid, a case study from Sumer et al. (2012) is considered. The soil and wave properties are listed in Table 1. A simple rectangular box is generated to represent the soil region. The length of the considered domain is equal to one wave length and the height is equal to soil depth *h*. The grid size used in this study is 100 x 20 with 100 cells in *x*- and 20 cells in *z*-direction. The time step is dt = 0.1 s. All selected values for the problem discretisation (time step and grid size) are based on convergence studies.

Figure 6 shows the progress of liquefaction front under the action of waves. By applying Biot consolidation equations and the pressure build-up equation, the liquefaction sets in after 7 seconds. The results show that the liquefaction begins from the mudline and progress downwards, thereby following the results provided by Sumer et al. (2012).

Table 1. Physical properties of the wave and seabed

Physical Property	***Value***	***Unit***
Soil depth *h*	0.4	m
Poisson ratio μ	0.29	-
Porosity n	0.51	-
Permeability k	1.5 x 10^{-5}	m/s
Elastic modulus E	5	MPa
Degree of saturation S_r	1	-
Emphrical constants[α_N β]	[0.174 -0.36]	-
Wave height H	0.18	m
Wave period T	1.6	s
Water depth d	0.55	m

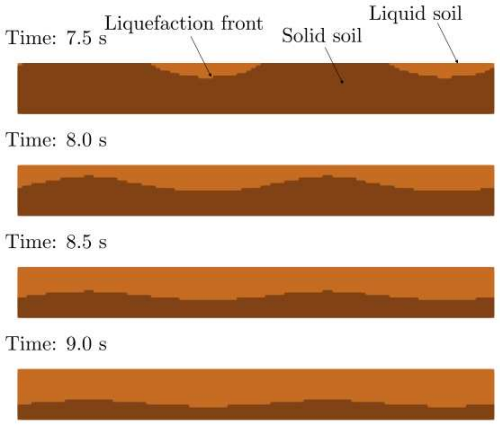

Figure 6: Example results of the propagation of the liquefaction front. The colour code serves as indicator: Dark brown refers to solid soil; light brown refers to liquefied soil.

6.3 Change of state: Liquid to solid

The same case study as mentioned in the previous Section 6.2 is considered to test the implementation for the change of state from liquid to solid soil. To that end, the simulation is restarted after 9.5 seconds with the wave pressure boundary being switched off. At that time instance, two-thirds of the seabed are liquefied. The liquefied soil is then allowed to settle without the waves. The additional properties are listed in Table 2.

Table 2. Physical properties required for the soil compaction

Physical Property	***Value***	***Unit***
Porosity of compacted soil n_c	0.354	-
Settling velocity V_0	0.0005	m/s
q (see Eq. (12))	2.7	-

Figure 7 shows the progress void ratio of soil grains α at four different time instances. The results show that, as the soil settles, the water molecules moves upwards due to the upward directed pressure gradient. Contrary, the soil settles down at the bottom, increasing the volume fraction of soil grains. This matches with the experimental observations in (Sumer et al., 2012), as the compaction front progress upwards from the impermeable base to the mudline.

7 CONCLUSIONS

This paper aims to presents the goals and initial results of the NuLIMAS project. Based on the presented results the following conclusions can be drawn:

(1) The entire sequence of seabed liquefaction can be expressed by a set of governing equations, enabling the implementation in OpenFOAM®.

(2) Initial numerical simulations for the pore pressure build-up, liquefaction, and compaction show promising results, comparing well with reference data from the literature. This forms a stepping stone for further calibration and validation against experimental results.

(3) Performing experiments for the calibration and validation of liquefaction is a complex task. The data acquired in the NuLIMAS framework provides a unique basis for the future analysis of liquefaction.

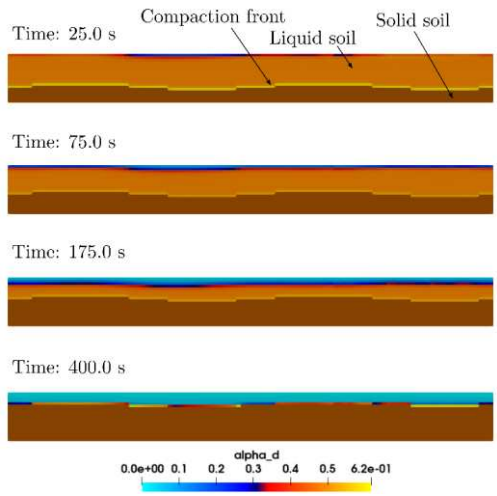

Figure 7: Example results of the compaction of the liquefied soil after waves are stopped to propagate. The colour code here refers to the void fraction of soil grains.

8 ACKNOWLEDGEMENTS

This work was supported within the ERA-NET Co-fund MarTERA Program under the H2020 Framework (Grant No. 728053), the German Federal Ministry for Economic Affairs and Climate Action (Grant No.03SX524A), the Scientific and Technological Research Council of Turkey (Grant No. TEYDEB-1509/9190068), and the Polish National Centre for Research and Development (Grant MarTERA-2/NuLIMAS/3/2021).

9 REFERENCES

Biot, M. (1941). General theory of three-dimensional consolidation. *Journal of applied physics*, pp. 155-164.

Bjerrum, J. (1973). Geotechnical problems invovled in foundations of structures in the North Sea. *Geotechnique*, 319-358.

De Alba, P., Chan, C., Seed, H. (1976). Sand liquefaction in large-scale simple shear tests. *Journal of the Geotechnical Engineering Division*, 909-927.

Dunn, S., Vun, P., Chan, A., Damgaard, J. (2006). Numerical modeling of wave-induced liquefaction around pipelines. *Journal of waterway, port, coastal, and ocean engineering*, 276-288.

Elsafti, H. and Oumeraci, H. (2016). A numerical hydro-geotechnical model for marine gravity structures. *Computers and Geotechnics*, 105-129.

Jeng, D. (2003). Wave-induced sea floor dynamic. *Applied Mechanics Reviews*, 407-429.

Jeng, D., Ye, J.-H., Zhang, J.-S., Liu, P.-F. (2013). An integrated model for the wave-induced seabed response around marine structures: Model verifications and applications. *Coastal Engineering*, 1-19.

Kazimierowicz-Frankowska, K., Kulczykowski, M., Majewski, D., Mierczyński, J., and Smyczyński, M. (2022). The effect of the height of the regular wave on seabed liquefaction. *Proceedings of the ASME 2022 41st International Conference on Ocean, Offshore and Artic Engineering*. Hamburg, Germany.

Li, J., and Jeng, D. (2008). Response of a porous seabed around breakwater heads. *Ocean Engineering*, 864-886.

Li, Y., Ong, M., Tang, T. (2020). A numerical toolbox for wave-induced seabed response analysis around marine structures in the OpenFOAM. *Ocean Engineering*, 106678.

Raman-Nair, W., Sabin, G. (1991). Wave-induced failure of poroelastic seabed slopes: A boundary element study. *Proceedings of the Institute of Civil Engineers*, 771-794.

Sakai, T. (1988). Effects of inertia and gravtiy on seabed response to ocean waves. *Modeling Soil-Water-Structure interactions*, 61-66.

Shanmugasundaram, R. K., Rusche, H., Windt, C., Kirca, V.S.O., Sumer, B M., Goseberg, N. (2022). Towards the Numerical Modelling of Residual Seabed Liquefaction Using OpenFOAM. *OpenFOAM Journal*, S. 94-115.

Stickle, M., De La Fuente, P., Oteo, C., Pastor, M., Dutto, P. (2013). A modelling framework for marine structure foundations with example application to vertical breakwater seaward tilt mechanism under breaking wave loads. *Ocean Engineering*, 155-167.

Sumer, B.M. (2014a). Advances in seabed liquefaction and its implications for marine structures. *Geotechnical Enigneering*, 2-14.

Sumer, B.M. (2014). *Liquefaction Around Marine Structure.* World Scientific.

Sumer, B.M. and Kirca, V.S.O. (2021). Scour and liquefaction issues for anchors and other subsea structures in floating offshore wind farms: A review. *Water Science and Engineering*, 3-14.

Sumer, B.M., Hatipoglu, F., Fredsoe, F., and Sumer, S.K. (2006). The sequence of sediment behaviour during wave induced liquefaction. *Sedimentology*, pp. 611-629.

Sumer, B.M., Kirca, V.S.O., Fredsoe, J. (2012). Experimental Validation of a Mathematical Model for Seabed Liquefaction Under Waves. *International Journal of Offshore and Polar Engineering*, 133–141.

Verruijt, A. (1969). Elastic sotrage of aquifers. *Flow through porous media*, S. 331-376.

Windt, C., Schimmels, S., Kudella, M., Shanmugasundaram, R., Rusche, H., Sumer, B., Kirca, V.S.O., Vanjakula, V. Adam, F., Majewski, D., Kazimierowicz-Frankowska, K. Hrycyna, G., Goseberg, N. (2022). Numerical modelling of liquefaction around marine structures – Progress and recent developments. *Proceedings of the ASME 41st International Conference on Ocean, Offshore and Arctic Engineering*. Hamburg, Germany.

Zhao, H., Jeng, D., Liao, C., Zhu, J. (2017). Three-dimensional modeling of wave-induced residual seabed response around a mono-pile foundation. *Coastal Engineering*, 1-21.

Zienkiewicz, O., Chang, C., Bettess, P. (1980). Drained, undrained, consolidating and dynamic behaviour assumptions in soils. *Geotechnique*, 385-395.